Geostandards and Geoanalytical Research (2023)

Online Supporting Information

Sources of inaccuracy in boron isotope measurement using LA-MC-ICP-MS

Jan **Fietzke**[1*] and Eleni **Anagnostou**[2]

GEOMAR Helmholtz Center for Ocean Research Kiel, Wischhofstr. 1-3, 24118 Kiel, Germany

[1] phone: +49 431 600 2106; email: jfietzke@geomar.de; ORCID: 0000-0002-5530-7208

[2] phone: +49 431 600 2312; email: eanagnostou@geomar.de; ORCID: 0000-0002-7200-4794

[*] Corresponding author.

Appendix S1: Preparation of epo-951 reference material

Boric acid NIST SRM 951 (aka NBS 951) has been established as the primary reference material for boron isotope measurements in the isotope geochemistry community. It appears tempting to facilitate it for LA-MC-ICP-MS, too. Unfortunately, because of two main reasons this is not practical and/or possible. One, it may be not desirable to have such a highly-concentrated source of boron placed inside of the ablation cell. Its B concentration exceeds that of typical samples and other reference materials by several orders of magnitude, and its presence and ablation could potentially result in contamination of other samples and produce high background levels of boron if not carefully controlled in its B release by the ablation. Two, and this is the more severe problem, crystalline boric acid appears almost impossible to be ablated in a sufficiently controlled way by 193nm UV laser radiation (at least for the ns laser systems used in this study). The laser radiation at this wavelength appears to not interact (no coupling) with crystalline boric acid.

Thus, we aimed for converting the NIST SRM 951 from its crystalline boric acid state into an easy to prepare and handle hard substrate, maintaining its primary boric acid isotope composition but being easy to scale in concentration and easy to ablate by 193 nm ns lasers.

200 mg of NIST SRM 951 were dissolved in 2 ml of methanol (freshly-opened bottle of Merck 99.9% methanol p.a.). This amount is well below the maximum solubility of boric acid in methanol ensuring its complete dissolution. 0.5 ml of this dissolved boric acid has been added to 10 ml of the resin (phase A) of two-component epoxy Araldite 2020. The mixing of the methanol with the resin has been performed by extensive pumping using a pipette (10 ml variable; set to 5 ml) until no visible streaks could be observed. 3 ml of the hardener (phase B) of Araldite 2020 have finally been added to

the mixture and mixed by pipette-pumping as described before. The final epoxy NIST SRM 951 blend was allowed to cure in two 10 ml ICP vials. The entire dissolution and mixing procedures have been performed in a clean-room environment.

After hardening of the epoxy resin had completed, the vials containing it had been cut to using a microtome saw. The resulting pellets are 14 mm in diameter and about 1 mm thick and referred to as epo-951 in the following text.

The whole procedure has been repeated without the addition of boric acid to allow for an estimation of the procedural blank.

Appendix S2: Chemical characterisation of boric acid epoxy pellet epo-951

Comparing the $^{11}B/^{12}C$ intensity ratios of both, the blank epoxy pellet and the epo-951 ablated under identical conditions, resulted in a relative boron procedural blank contribution of 7.2e-5 +- 9.6e-5 (95% conf.), insignificant in its potential to alter the isotopic composition.

Repeated measurements of silicate glass reference material NIST SRM 610 vs. epo-951 using the AXIOM MC-ICP-MS, in multi-ion-counting mode and under hot plasma conditions (NAI of 15), resulted in NIST SRM 610 $\delta^{11}B$ = 0.06 ± 0.22 ‰ (95% conf., *n* = 130). This result agrees with the most precise published TIMS data of $\delta^{11}B$ = 0.0 ± 0.3 ‰ (2*s*) (Jochum *et al*. 2011), confirming that NIST SRM 610 is practically indistinguishable from NIST SRM 951 boric acid reference material with respect to its boron isotope composition. We thus consider the epo-951 to be an unbiased representation of the isotopic composition of NIST SRM 951.

Preliminary boron concentration estimates for epo-951 resulted in B/C = 448 ± 11 µmol/mol (2*s*, *n* = 4). The estimate is based on B/Ca concentration LA-ICP-MS measurements of a skeletal area of a natural *D. dianthus* sample using NIST SRM 610 as calibration material (reference concentration B/Ca = 350 µg/g equalling 15926 µmol/mol, Jochum *et al*. 2011) and the approximation of a carbon to calcium molar ratio of 1 in the *D. dianthus* skeletal aragonite. The resulting B/C molar ratio of the *D. dianthus* sample and its measured B/C intensity ratios have been used to convert the B/C intensity ratios measured in the epo-951 into B/C molar ratios for the later. The quality of the LA-ICP-MS B/Ca concentration measurements via NIST SRM 610 has been evaluated by repeated measurements of carbonate reference material JCp-1 and JCt-1, yielding mean results of 459 ± 12 µmol/mol (95% conf., *n* = 7) for JCp-1 and 204 ± 6 µmol/mol (95% conf., *n* = 7) for JCt-1, respectively, both in good agreement with published data (Hathorne *et al*. 2013).

The chemical composition of epo-951, thus, makes it a useful Ca-free, homogeneous, easy to ablate boron isotope representation of the NIST SRM 951 boric acid reference material. The preparation procedure described above is also scalable, i.e. it can be easily modified to allow for customizing the boron concentration of an epoxy pellet if required by the application.

Appendix S3: Overview of possible contributions to inaccuracies in B isotope LA-MC-ICP-MS measurement

In this section we provide two examples illustrating our approach in conceptualizing analytical problems. Both remain intentionally in their raw unedited version to allow for an unbiased look into the actual process. The first is a mind map (Figure S1), which has been prepared as a ppt file, but any other tool would be fine, too. Its purpose had been to help focus on the actual measurement process, guided by the questions:

- What happens to the sample at which point? and
- What impacts the "translation" of the sample's chemical into spectral information?

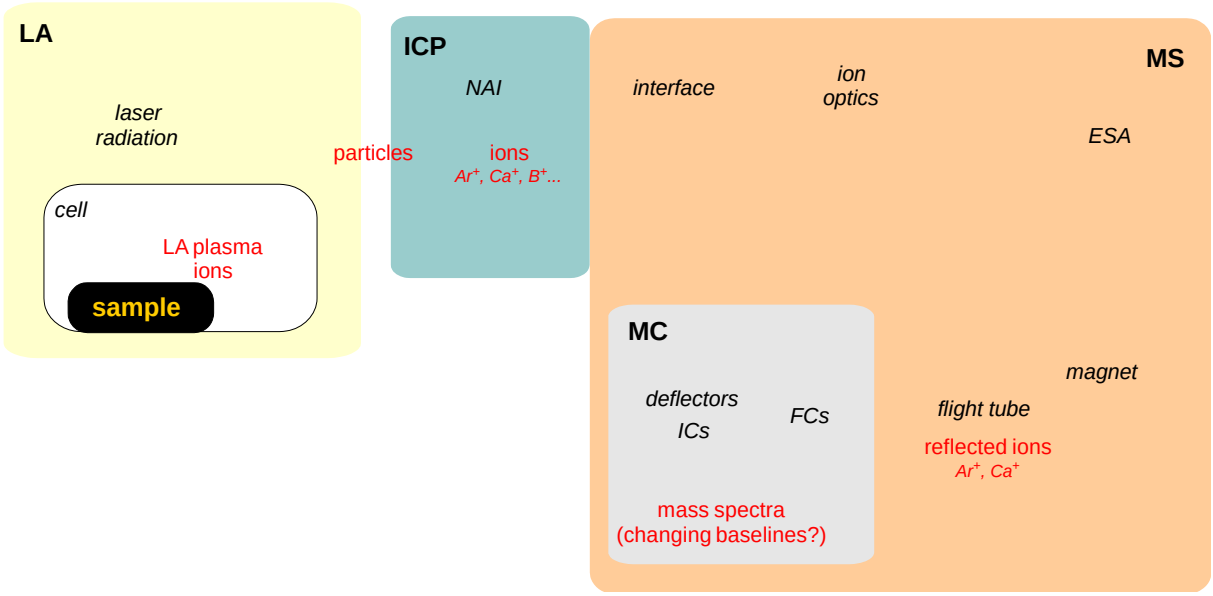

Figure S1: Mind map: Systematic of the components and likely effects involved in LA-MC-ICP-MS measurement of boron isotopes.

The second is a list collecting ideas while going through the mind map (Figure S1). It is simply a collection of items that came to mind taking the perspective of the sample, making its "journey" from the ablation chamber to its ultimate representation of spectral information.

List of potential issues:

- Sample: (surface contamination, incl. redeposition)
- LA: elemental/mass fractionation (mostly during condensation after expansion/cooling of material from LA plasma, link to down-hole fractionation)
- Transfer of particles to ICP (fractionation during transport mostly from differences in particle size/density plus gas vs. particle)
- ICP: NAI-dependent production of B+, Ca+, Ar+ etc., impact on elemental sensitivity, mass-load related impact on NAI, formation of Ca4+ possible? Most likely not, considering the 4^{th}IP's of Ar (59.8 eV) vs. Ca (67.3 eV) and signal intensities of Ar+ and Ca+
- Interface: mass fractionation and transmission (NAI-dependent, most likely impacted by cone design and interface pressure)

- Ion optics: optimized for specific material, optimum depends on NAI, if mass load impacts NAI focus changes
- ESA: potentially impacted by changing NAI, ion energy impacted
- Magnet/flight tube: same as ESA, potential reflection of Ar+ and Ca+ from flight tube design, when magnet is set to allow for transmission of B ions, high intensity ion beams of Ar and Ca may hit flight tube wall at some point due to the trajectories of the about 4× heavier than B, Ar and Ca ions
- MC: scattered ion background at focal plane of FCs (depending on Ar, Ca and NAI), preventable if deflectors separate B ions from scattered ions (different angle) on their way to ICs, consider difference in detection efficiency for multiply charged ions: IC counts ions, FC collects charge (e.g. Ar^{4+} measured on FC one ion = 4× the charge)

Again, both, mind map and list, have not been heavily edited after their initial preparation. They are by no means exhaustive or complete.

Appendix S4: Additional information regarding test data

Typical operating parameters for the different instruments used in this study are provided in Table S1.

MC-ICP-MS instrument	**Operating parameter**
AXIOM	cool gas [l/min]: 17 aux gas [l/min]: 0.8 laser cell gas [l/min]: 0.7 (He) rf power [W]: 1000 sample gas [l/min]/*NAI*: 0.55/*19.0* 0.60/*12.7* 0.65/*7.8* 0.70/*3.9* 0.75/*1.7* 0.80/*0.7* 0.85/*0.3*
Neptune plus	cool gas [l/min]: 17 aux gas [l/min]: 0.8 laser cell gas [l/min]: 1.0 (He) rf power [W]: 1000 sample gas [l/min]/*NAI*: 0.7/*3* 0.75/*2* 0.8/*1.3* 0.85/*0.8* 0.9/*0.4* rf power [W]: 1200 sample gas [l/min]/*NAI*: 0.73/*6.7* 0.775/*4.8* 0.825/*3.0* 0.875/*1.9* 0.925/*1.1* 0.975/*0.6*

	0.987/*0.5* 1.025/*0.3*
Nu Plasma3	cool gas [l/min]: 16 aux gas [l/min]: 0.8 laser cell gas [l/min]: 1.0 (He) rf power [W]: 1000 sample gas [l/min]/*NAI*: 0.54/*17.8* 0.60/*10.9* 0.65/*7.3* 0.70/*4.2* 0.75/*2.4* 0.80/1.*4* 0.85/*0.7* 0.90/*0.4* 0.95/*0.2*

Table S1: Operating parameters for the different MC-ICP-MS types used in this study.

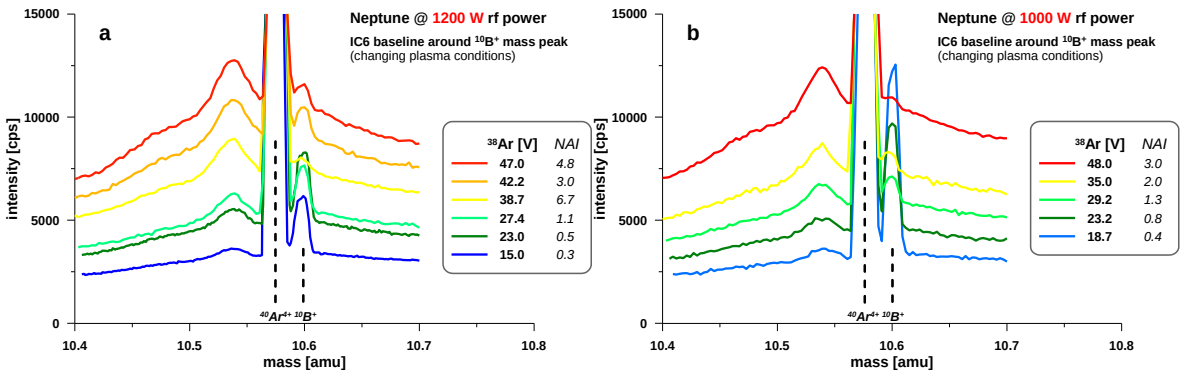

Figure S2: Spectral baseline scans measured on IC6 under different plasma condition (a: 1200 W rf test series; b: 1000 W rf test series). Note, the higher ^{10}B in the 1000 W test series are a result of elevated B backgrounds from intense ablations done during the test.

As reported in the main text and Figure 1 for the 1200 W rf series of experiments the shape of the spectral baseline around the ^{10}B peak is fairly stable and scales with the intensity of ^{38}Ar beam which

in and of itself depends on the plasma condition (NAI). A similar experiment using 1000 W rf power confirms the behaviour observed at 1200 W rf power (Figure S2), resulting in the common baseline *vs*. ^{38}Ar trend displayed in Figure 2 (main text).

Additionally, the peak baseline intensities (10.54 amu) are tightly correlated to the baseline measured at the position for data collected on IC6 during regular B isotope measurements (10.505 amu) (see Figure S3).

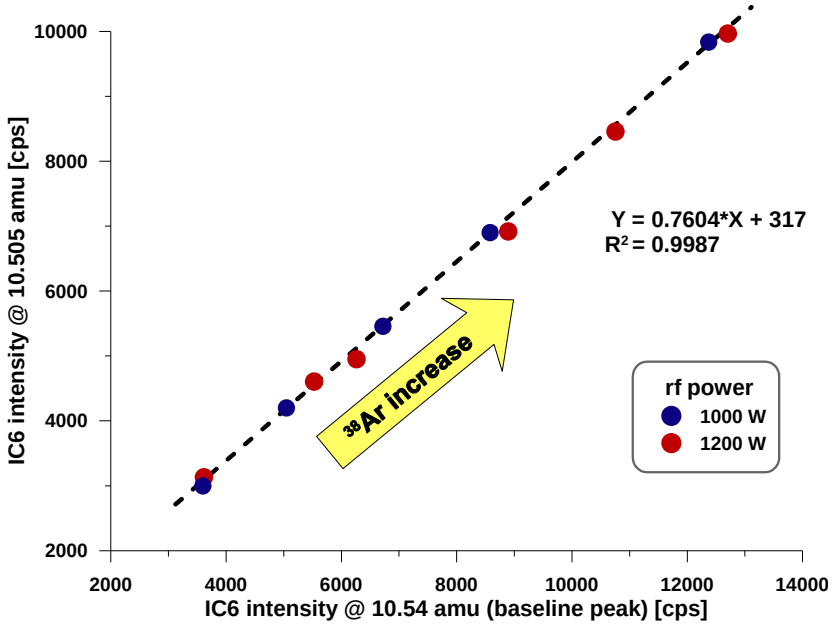

Figure S3: Correlation between baseline intensity measured at 10.505 amu (IC6 spectral position during B isotope Faraday cup multi-collection) and IC6 baseline peak intensity at 10.54 amu. Data represent 6 (1200 W rf tests) respectively five different plasma condition (1000 W rf tests). Both tests' baseline intensities are responding in a common way linearly following the increase in ^{38}Ar.

We take this as an indication that indeed the baseline is only scaling, but not changing its shape. This implies that both positions (10.505 amu and 10.54 amu) are equally good representations of the baseline and useable for correcting B isotope data for changing baselines.

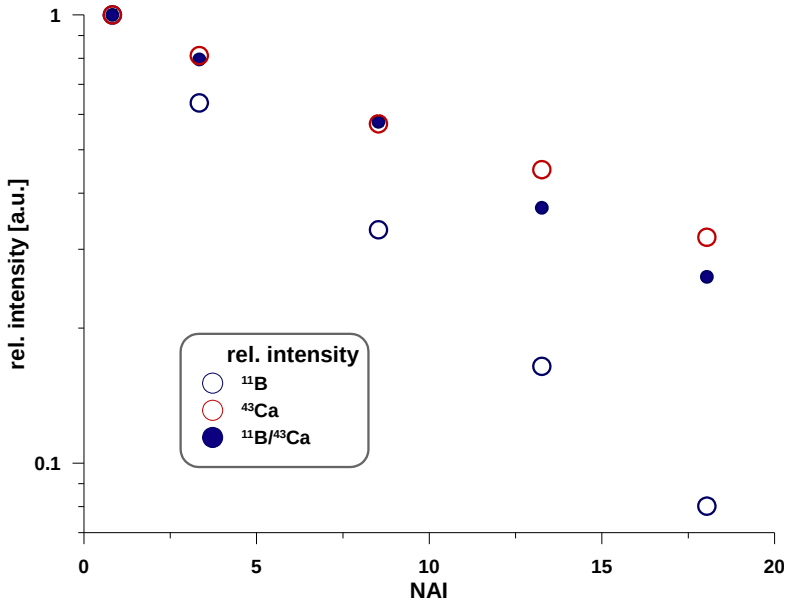

Figure S4: Changes in relative signal intensity of ^{11}B and ^{43}Ca and the relative sensitivity ratio $^{11}B/^{43}Ca$ depending on plasma condition (NAI). Measured using AXIOM MC-ICP-MS ablating NIST SRM 610.

Since both, Ar and Ca ions, contribute to the scattered ion baseline it is noteworthy to consider the changes in B and Ca intensity, when ablating the same material at different plasma conditions. In Figure S4 an example is provided using identical ablation parameters for NIST SRM 610 using the AXIOM MC-ICP-MS tuned for different NAI. The declines of both ^{11}B and ^{43}Ca signal intensities, follow trends, which closely resemble exponential decays of intensity with increasing NAI. For ^{11}B, however, the decay (~ $e^{-0.14*NAI}$) is systematically stronger than for ^{43}Ca (~ $e^{-0.06*NAI}$). In our opinion this can be interpreted again in the framework provided by the RDM model. Instrumental mass fractionation caused by preferential diffusive loss of lighter ions from the core of the plasma impacts ^{11}B relatively stronger than ^{43}Ca. The loss itself follows a systematic which comes close to a 1/m relationship, e.g., at NAI of 18, ^{11}B has declined to ~ 8% and ^{43}Ca to ~ 32% of its respective peak intensity at NAI ~ 0.6.

To illustrate the differences in the scattered ion background for the three types of MC-ICP-MS used in this study and in particular the respective impact by the use of ion counters with beam deflectors vs. Faraday cups we provide background signal intensity scans in Figure S5. As can be seen in Figure S5 for all instruments the background measured using Faraday cups is effectively suppressed when ion counters with beam deflection are used. If ion counters without beam deflection are used (Neptune plus) there is no such suppression of the scattered ion background.

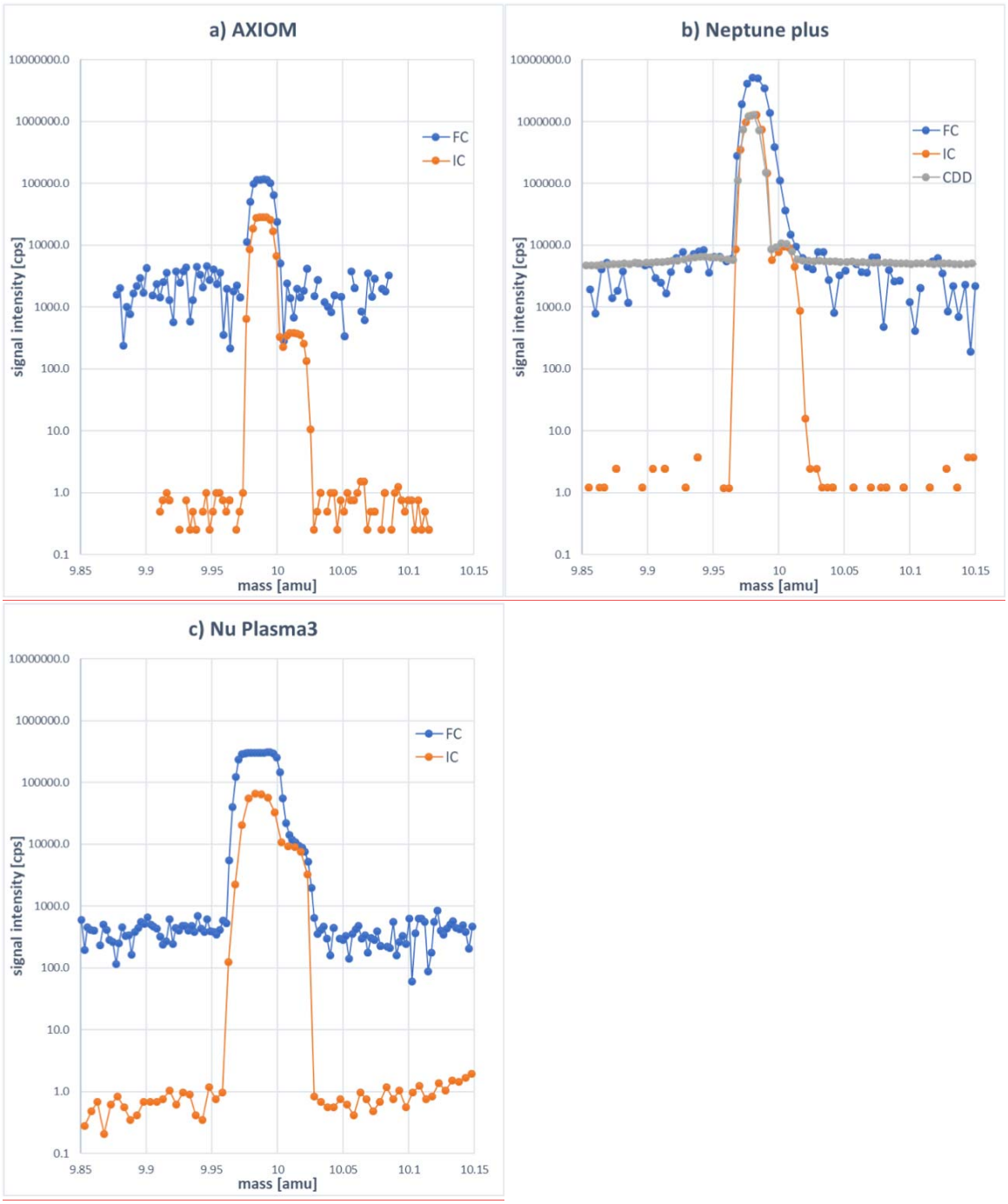

Figure S5: Examples of background signal intensities mass scans around 10 amu for (a) AXIOM, (b) Neptune plus and (c) Nu Plasma3 using Faraday cups or ion counters (IC). All signal intensities measured as voltages using Faraday cups have been converted into the equivalent in counts per second (cps) for better comparability. For each instrument the use of beam deflectors for IC measurements resulted in a strong background suppression. For ion counters without beam deflectors (CDD in Neptune plus) no such background suppression can be observed.

Appendix S5: Release and Diffusion Model (RDM)

A release and diffusion model (RDM) has been set up in Excel. It consists of 39 × 39 × 400 cells [X;Y;Z]. The main features are the gradual release of B along the centre *Z* axis and a layer by layer diffusion along Z. While the release of B does not differentiate between the two boron isotopes, the diffusive iteration along Z is calculated separately for ^{10}B and ^{11}B. For each cell, the isotope ratios can be calculated from the 3D abundance distributions of the two isotopes.

The release is represented by a Gaussian distribution centred at *Z* = 200. The σ of the function can be modified to modify the rate of release. The release function is normalized to 1 to represent complete B release within the Z boundaries. The latter for obvious reasons limits the range of acceptable σ to exclude unrealistic start and end properties. Figure S6 provides one example release function.

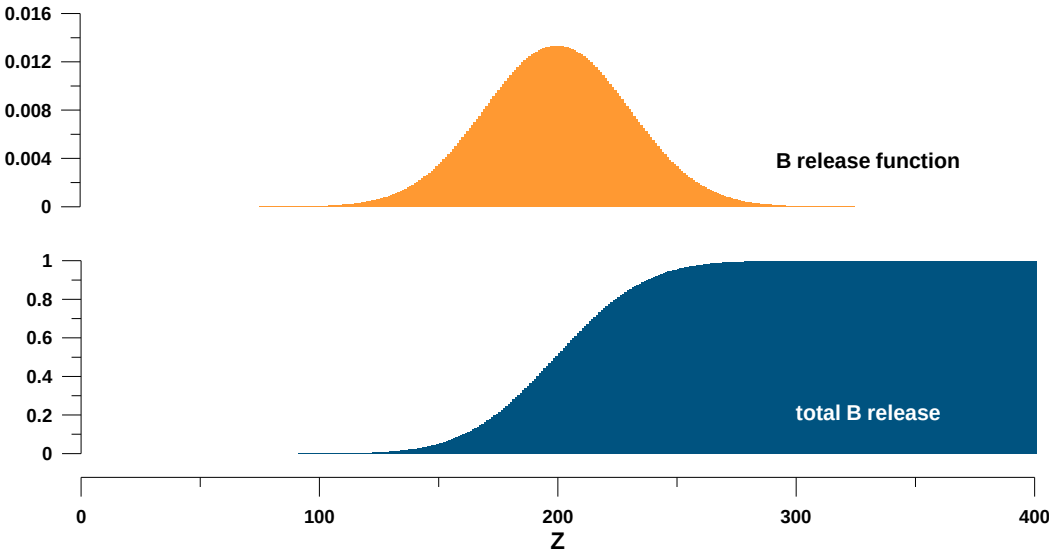

Figure S6: Example of a release function used in the model runs, a Gaussian centred at Z = 200 and a σ of 30. The function is normalised to provide a total B release of 1 at max Z.

To allow for a more realistic release feature in the model, the release function is not solely applied to the centre cell in the respective [X;Y] layer, which would only represent ~ 0.5 × 0.5 mm. Instead, the release is performed over 3 × 3 cells, allocating 25% of the particular release to the centre cell, 12.5% to each of the neighbouring four side cells and 6.25% to each of the 4 corner cells. This release is applied to both isotopes in an identical way.

Starting at 0 in all Z = 0 cells the model runs separately for ^{10}B and ^{11}B in a similar way to produce layer by layer the cell contents of the respective isotope. Diffusion is simulated by a simplified Gaussian smoothing function. This approach redistributes the content of the cells in layer Z into the 3 × 3 cells in layer Z+1. This procedure is illustrated in Figure S7. The parameter D driving the smoothing/diffusion is mass-dependent, i.e., 10% higher for the ^{11}B compared with ^{10}B. The redistribution factors in the Z+1 layer are normalised to 1 for material conversation. The material release is added into each layer according to the above-mentioned release function spread over the centre 3 × 3 cells.

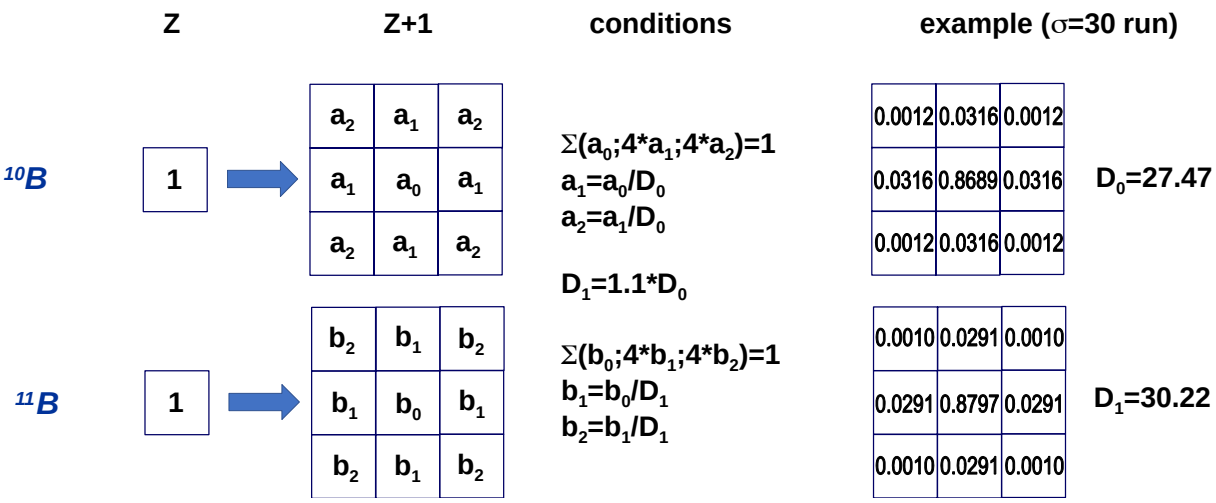

Figure S7: Calculating systematic for the step from layer Z to Z+1 to simulate the mass-dependent diffusion of ^{10}B and ^{11}B. The relative mass difference, is rounded to 1.1 based on the ratio of the boron isotope masses of 1.0995. The example provided stems from one model run used in the study.

Once a release function is defined the model only has one adjustable parameter left. This is the diffusion parameter D_0. It can be adjusted to match the model's fractionation result for the point of maximum B intensity. It is based on two experimental observations. The first is the NAI of ~ 0.6 for maximum B intensity (see Figure S4). The second is based on the trends of relative B isotope fractionation *vs*. NAI (Figure S8). This trend is based on interpolating the data displayed in Figure 5, normalising the boron isotope fractionation to the respective maximum measured ratios (using the clogged and open cone AXIOM data).

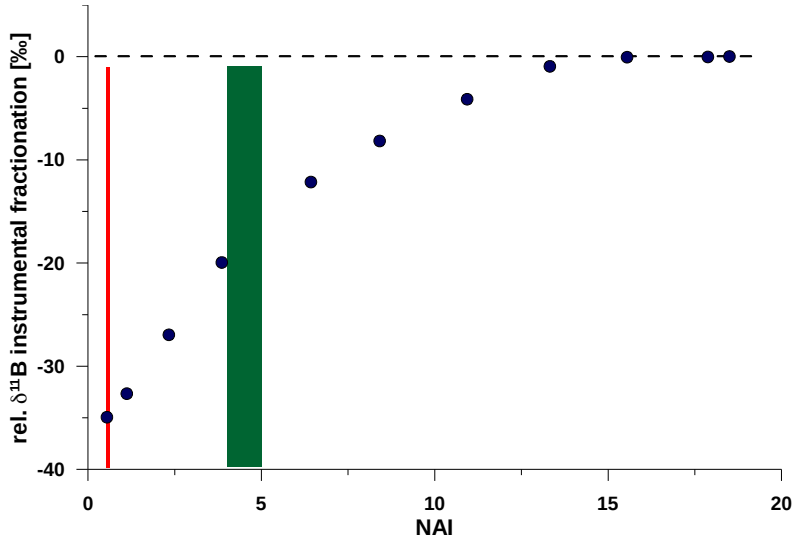

Figure S8: Trend of relative boron isotope fractionation vs. NAI. The data are interpolated from the two data sets obtained using the AXIOM (see Figure 6, main text), calculated relative to the heaviest measured boron ratios (high-NAI endpoints). Red line marks the NAI = 0.6 experiment (maximum B sensitivity), green square indicates the NAI range of 4–5, i.e. the experimentally determined threshold for vanishing matrix-dependent offsets (see Figure 5, main text).

For NAI = 0.6 (maximum B sensitivity) we obtain a relative boron isotope fractionation of ~ -35‰. At NAI of 4–5 (the minimum for negligible matrix-offsets) the fractionation is half of the NAI 0.6 (~ -17.5‰).

In the model we use the estimate of -35‰ fractionation (relative to hot end at max Z) for maximum B sensitivity. The diffusion parameter D_0 is iteratively adjusted to result in -35‰ fractionation for the model cell of maximum B signal intensity.

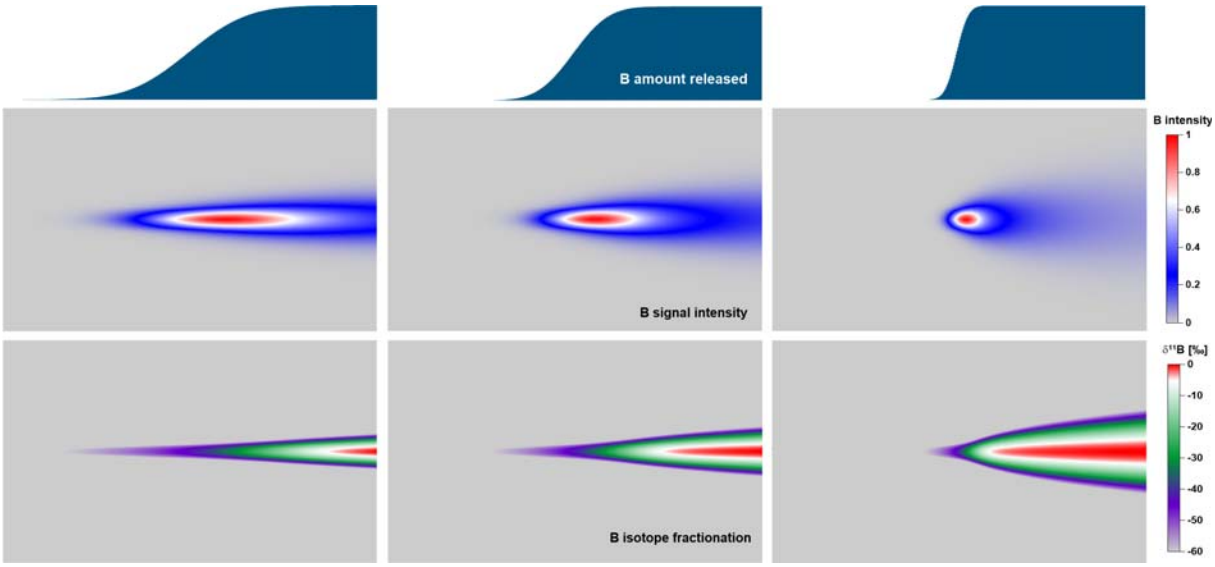

Figure S9: Release and diffusion model (RDM) results using three different release functions, all centred at Z = 200, but with σ equal to 50 (left), 30 (middle) and 10 (right panels).

In Figure S9 three example runs of the model using slightly different release functions are displayed. The main impact of the shape of the release function can be observed in stretching/contraction of the overall trends in intensity and isotope fractionation. Nevertheless, the overall systematic between B release and fractionation is only impacted to a small degree (see Figure S10). For the three selected release functions the RDM estimate for the B amount released at the NAI of negligible matrix-dependent offsets (rel. fractionation of -17.5‰) is 97–97.5%.

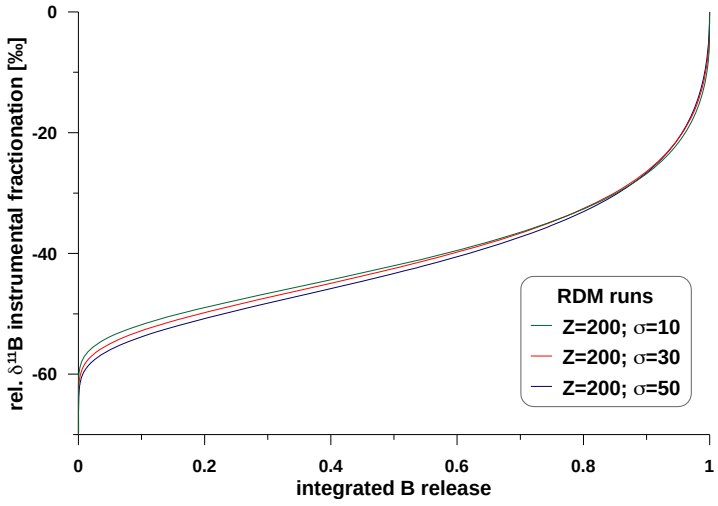

Figure S10. Trends of boron isotope fractionation vs. B release for the three RDM runs displayed in Figure S8.

References

Hathorne E.C., Gagnon A., Felis T., Adkins J., Asami R., Boer W., Caillon N., Case D., Cobb K.M., Douville E., deMenocal P., Eisenhauer A., Garbe-Schönberg D., Geibert W., Goldstein S., Inoue M., Kawahata H., Kölling M., Cornec F.L., Linsley B.K., McGregor H.V., Montagna P., Nurhati I.S., Quinn T.M., Raddatz J., Rebaubier H., Robinson L., Sadekov A., Sherrell R., Sinclair D., Tudhope A.W., Wei G., Wong H., Wu H.C. and You C.F. (2013)
Interlaboratory study for coral Sr/Ca and other element/Ca ratio measurements. **Geochemistry Geophysics Geosystems, 14 (9),** 3730-3750.

Jochum K.P., Weis U., Stoll B., Kuzmin D., Yang Q., Raczek I., Jacob D.E., Stracke A., Birbaum K., Frick D.A., Günther D. and Enzweiler J. (2011)
Determination of reference values for NIST SRM 610–617 glasses following ISO guidelines. **Geostandards and Geoanalytical Research, 35 (4),** 397-429.